Using a One-Electron Shuttle for the Multielectron Reduction of CO₂ to Methanol: Kinetic, Mechanistic, and Structural Insights

Emily Barton Cole, Prasad S. Lakkaraju,[†] David M. Rampulla, Amanda J. Morris,
Esta Abelev, and Andrew B. Bocarsly*

Department of Chemistry, Princeton University, Princeton, New Jersey 08544

Received March 29, 2010; E-mail: bocarsly@princeton.edu

Abstract: Pyridinium and its substituted derivatives are effective and stable homogeneous electrocatalysts for the aqueous multiple-electron, multiple-proton reduction of carbon dioxide to products such as formic acid, formaldehyde, and methanol. Importantly, high faradaic yields for methanol have been observed in both electrochemical and photoelectrochemical systems at low reaction overpotentials. Herein, we report the detailed mechanism of pyridinium-catalyzed CO₂ reduction to methanol. At metal electrodes, formic acid and formaldehyde were observed to be intermediate products along the pathway to the 6e⁻-reduced product of methanol, with the pyridinium radical playing a role in the reduction of both intermediate products. It has previously been thought that metal-derived multielectron transfer was necessary to achieve highly reduced products such as methanol. Surprisingly, this simple organic molecule is found to be capable of reducing many different chemical species en route to methanol through six sequential electron transfers instead of metal-based multielectron transfer. We show evidence for the mechanism of the reduction proceeding through various coordinative interactions between the pyridinium radical and carbon dioxide, formaldehyde, and related species. This suggests an inner-sphere-type electron transfer from the pyridinium radical to the substrate for various mechanistic steps where the pyridinium radical covalently binds to intermediates and radical species. These mechanistic insights should aid the development of more efficient and selective catalysts for the reduction of carbon dioxide to the desired products.

Introduction

The electrochemical reduction of carbon dioxide (CO₂) has generated substantial interest over the past decade as a way to potentially convert this greenhouse gas into useful fuels and small organics. Most electrochemical[1-5] and photoelectrochemical[6,7] systems for the reduction of CO₂, however, produce only the 2e⁻ reduction products of CO and formate. There have been fewer

reports on the further reduction of CO₂ to products such as methane, methanol, and ethanol, to name a few. Typically, systems reported to yield such products either require extensive energy input to overcome kinetic barriers or possess poor stability. The main limitation in achieving such products has been attributed to the inability of most catalysts to effect multielectron transfers along with the required multiproton transfers.[8-10] In order to produce higher order products, there has been a focus on transition-metal-based electrocatalysts containing multiple metal centers to facilitate multielectron transfers. This approach is based on the concept that a multielectron mechanism is required to produce highly reduced species.[11-13] However, while multielectron charge-transfer catalysts have been demonstrated to effect the 2e⁻ reduction of

[†] Also at Georgian Court University, Lakewood, NJ 08701.

(1) Dubois, D. L. Electrochemical Reactions of Carbon Dioxide. In *Encyclopedia of Electrochemistry*; Bard, A. J., Stratmann, M., Eds.; Wiley-VCH Verlag GmbH & Co. KGaA: Weinheim, 2006; pp 202–225.

(2) Frese, J. K. W. Electrochemical Reduction of CO₂ at Solid Electrodes. In *Electrochemical and Electrocatalytic Reactions of Carbon Dioxide*; Sullivan, B. P., Krist, K., Guard, H. E., Eds.; Elsevier: Amsterdam, 1993; pp 145–216.

(3) Halmann, M. M.; Steinberg, M. Electrochemical Reduction of CO₂. In *Greenhouse Gas Carbon Dioxide Mitigation: Science and Technology*; Halmann, M. M., Steinberg, M., Eds.; Lewis Publishers: Boca Raton, FL, 1999; pp 411–515.

(4) Hori, Y. Electrochemical CO₂ Reduction on Metal Electrodes. In *Modern Aspects of Electrochemistry*; Vayenas, C. G., White, R. E., Gamboa-Aldeco, M. E., Eds.; Springer: New York, 2008; Vol. 42, pp 89–189.

(5) Taniguchi, I., Electrochemical and Photoelectrochemical Reduction of Carbon Dioxide. In *Modern Aspects of Electrochemistry*; Bockris, J. M., Conway, B. E., White, R. E., Eds.; Springer: New York, 1989; Vol. 20, pp 327–400.

(6) Halmann, M. M.; Steinberg, M. Photoelectrochemical Reduction of CO₂. In *Greenhouse Gas Carbon Dioxide Mitigation: Science and Technology*; Halmann, M. M., Steinberg, M., Eds.; Lewis Publishers: Boca Raton, FL, 1999; pp 517–527.

(7) Lewis, N. S.; Shreve, G. A. Photochemical and Photoelectrochemical Reduction of Carbon Dioxide. In *Electrochemical and Electrocatalytic Reactions of Carbon Dioxide*; Sullivan, B. P., Krist, K., Guard, H. E., Eds.; Elsevier: Amsterdam, 1993; pp 263–289.

(8) Heinze, K.; Hempel, K.; Beckmann, M. *Eur. J. Inorg. Chem.* **2006**, 2040–2050.

(9) Heyduk, A. F.; Macintosh, A. M.; Nocera, D. G. *J. Am. Chem. Soc.* **1999**, *121*, 5023–5032.

(10) Rosenthal, J.; Bachman, J.; Dempsey, J. L.; Esswein, A. J.; Gray, T. G.; Hodgkiss, J. M.; Manke, D. R.; Luckett, T. D.; Pistorio, B. J.; Veige, A. S.; Nocera, D. G. *Coord. Chem. Rev.* **2005**, *249*, 1316–1326.

(11) Bian, Z.-Y.; Sumi, K.; Furue, M.; Sato, S.; Koike, K.; Ishitani, O. *Inorg. Chem.* **2008**, 10801–10803.

(12) Tanaka, K.; Ooyama, D. *Coord. Chem. Rev.* **2002**, *226*, 211–218.

(13) Toyohara, K.; Nagao, H.; Mizukawa, T.; Tanaka, K. *Inorg. Chem.* **1995**, *34*, 5399–5400.

CO$_2$ to CO and formate, more highly reduced products are only sporadically observed.

We have previously described the electrochemical reduction of CO$_2$ to the 6e$^-$ reduction product of methanol catalyzed by a simple one-electron electrocatalyst, the pyridinium cation.[14] At hydrogenated Pd electrodes, faradaic efficiencies for the reduction of CO$_2$ to methanol of ~30% were observed at overpotentials of only ~200 mV. Cyclic voltammetric analysis showed a square root dependence of scan rate on peak current density, indicating that pyridinium is a solution-dissolved species that must diffuse to the electrode interface. Trace levels of formaldehyde were also observed as a CO$_2$ reduction product. It is now found that formic acid, formaldehyde, and methanol are all products in the electrochemical-based pyridinium system. More recently, we have exported this chemistry to a p-GaP photoelectrochemical system to yield nearly 100% faradaic efficiency for methanol at underpotentials as high as 300 mV below the thermodynamic potential of -0.52 V vs SCE at our system pH of 5.2.[15] No other products were detected. To our knowledge, this is the first system capable of reducing CO$_2$ to methanol using only light energy.

While there are reports in the literature on electrochemical[16−23] and photoelectrochemical[24−26] systems capable of reducing CO$_2$ to methanol, there has been limited effort aimed at determining the mechanisms[23,25,27] of reduction for the various catalysts and electrode materials, including the pyridinium-catalyzed reduction we have reported. In order to develop an efficient and selective system for methanol production, the mechanism of such processes must be determined. Here, the detailed mechanism of pyridinium-catalyzed CO$_2$ reduction to the products formic acid, formaldehyde, and methanol is investigated. Using various analytical electrochemical techniques, simulations of cyclic voltammograms (CVs), molecular orbital calculations, and NMR studies using ^{13}C- and ^{15}N-enriched samples, we were able to gain insights into the crucial steps leading to the various products and intermediates and ultimately to methanol. Perhaps our most important finding is that this simple one-electron charge-transfer catalyst is able to efficiently effect at least four of the six total electron transfers necessary in the formation of methanol. That is, the mechanism of reduction appears to occur through multiple single-electron transfers, offering a metal-free catalyst alternative for CO$_2$ transformation into highly reduced species.

The complete reduction of CO$_2$ to methanol through formic acid and formaldehyde intermediates is a complicated mecha-

nism. Therefore, we first evaluated the electrochemical behavior of the pyridinium catalyst in the absence of CO$_2$ and the generation of the active CO$_2$ reducing species, the pyridinium radical. For our mechanistic studies we have chosen to kinetically model all the reduction steps presented here at a platinum electrode due to the reversible nature of pyridinium reduction at this interface.

The data obtained indicate that the complete reduction of CO$_2$ to the 6e$^-$-reduced product of methanol goes sequentially through the 2e$^-$- and 4e$^-$-reduced intermediates formic acid and formaldehyde, respectively. Therefore, the overall mechanism is discussed on the basis of the separate 2e$^-$ reductions of CO$_2$ to formic acid, formic acid to formaldehyde, and finally formaldehyde to methanol. While overall the mechanism we provide is best typified as a globally homogeneous process, as discussed in the following sections, there are specific aspects of the proposed mechanism that are surface-sensitive. The specifics of the surface interactions have not been elucidated at this time and are the subject of ongoing investigation. To date, we have studied a variety of pyridine analogues and the effects of substituent groups on electrochemical behavior and product yields. Herein, a limited set of pyridine derivatives is examined, with a focus on pyridine and 4-*tert*-butylpyridine. These two catalysts were selected because the same rate-limiting step for the overall reduction of CO$_2$ to methanol was observed for both of them. The comparison thus allows for a validation of the proposed mechanism and the presence of key reaction intermediates.

Results and Discussion

Pyridinium Charge Transfer and Hydrogen Generation in the Absence of CO$_2$. In aqueous acidic solution, pyridine is protonated to yield the electroactive pyridinium cation shown in reaction 1.

$$\text{(reaction 1)} \qquad K_a = 6.76 \times 10^{-6} \qquad (1)$$
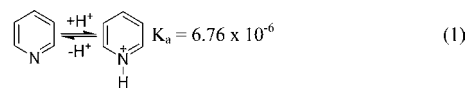
The aqueous reduction of pyridinium to the pyridinium radical has been reported to proceed as a 1e$^-$ reduction coupled to the catalytic generation of hydrogen, which follows the EC′ (an electrochemical step followed by a catalytic chemical reaction that regenerates the electrocatalyst)-type mechanism shown in reactions 2 and 3.[28]

$$\text{(reaction 2)} \qquad (E^\circ, \alpha, k_{\text{et}}) \qquad (2)$$

$$\text{(reaction 3)} \qquad (3)$$
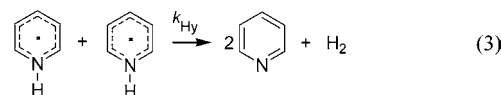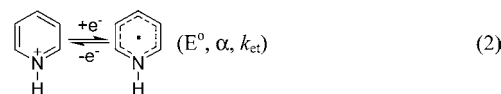
The electrochemical constants (E°, α, k_{et}) and kinetic parameters (k_{Hy}) for the reduction of pyridinium and 4-*tert*-butylpyridinium in the absence of CO$_2$, reported in Table 1, represent average values obtained by fitting experimental CVs over the scan rate range from 1 mV/s to 1 V/s to reactions 1−3. The fitting program was allowed to estimate the concentration

(14) Seshadri, G.; Lin, C.; Bocarsly, A. B. *J. Electroanal. Chem.* **1994**, *372*, 145–150.

(15) Barton, E. E.; Rampulla, D. M.; Bocarsly, A. B. *J. Am. Chem. Soc.* **2008**, *130*, 6342–6344.

(16) Bandi, A.; Kuhne, H. *J. Electrochem. Soc.* **1992**, *139*, 1605–1610.

(17) Frese, K.; Leach, S. *J. Electrochem. Soc.* **1985**, *132*, 259–260.

(18) Li, J.; Prentice, G. *J. Electrochem. Soc.* **1997**, *144*, 4284–4288.

(19) Ohkawa, K.; Noguchi, Y.; Nakayama, S.; Hashimoto, K.; Fujishima, A. *J. Electroanal. Chem.* **1994**, *367*, 165–173.

(20) Popic, J.; AvramovIvic, M.; Vukovic, N. *J. Electroanal. Chem.* **1997**, *421*, 105–110.

(21) Qu, J.; Zhang, X.; Wang, Y.; Xie, C. *Electrochim. Acta* **2005**, *50*, 3576–3580.

(22) Summers, D.; Leach, S.; Frese, K. *J. Electroanal. Chem.* **1986**, *205*, 219–232.

(23) Watanabe, M.; Shibata, M.; Kato, A.; Azuma, M.; Sakata, T. *J. Electrochem. Soc.* **1991**, *138*, 3382–3389.

(24) Aurian-Blajeni, B.; Halmann, M.; Manassen, J. *Sol. Energy Mater.* **1983**, *8*, 425–440.

(25) Canfield, D.; Frese, J. K. W. *J. Electrochem. Soc.* **1983**, *130*, 1772–1773.

(26) Halmann, M. *Nature* **1978**, *275*, 115–116.

(27) Ogura, K.; Takagi, M. *J. Electroanal. Chem.* **1986**, *206*, 209–216.

(28) Baumgartel, H.; Retzlav, K.-J. Heteroaromatic Compounds. In *Encyclopedia of Electrochemistry of the Elements*; Bard, A. J., Lund, H., Eds.; Marcel Dekker: New York, 1984; Vol. XV, p 194.

Table 1. Standard Potentials, Kinetic Constants,[a] and pK_a Values for the Electrochemical Reduction of Pyridinium and 4-*tert*-Butylpyridinium and Catalyzed Hydrogen Generation

electrocatalyst	pK_a	$E°$ (V)[b]	α	k_{et} (cm s^{-1})[c]	k_{Hy} (M^{-1} s^{-1})[d]
pyridinium	5.17	−0.58	0.64	0.010	2.9$_5$
4-*tert*-butylpyridinium	6.2	−0.62	0.46	0.0053	1.5

[a] Simulations including reactions 1−3. [b] All potentials referenced to the SCE. [c] Reaction 2. [d] Reaction 3.
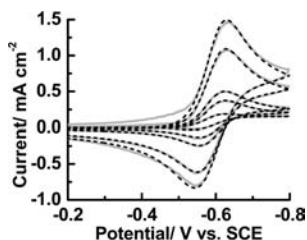
Figure 1. Comparison of experimental (solid) and simulated (dash) CVs for the reduction of pyridinium in aqueous solution at pH 5.3 with 0.5 M KCl as supporting electrolyte. Scan rates of 1, 5, 10, 50, and 100 mV/s are shown. The working electrode was a Pt disk (area = 0.13 cm²), polished using 1 μm alumina and sonicated in deionized water prior to use.

of pyridinium present at the electrode−electrolyte interface according to reaction 1. The calculated concentrations were consistent with the values estimated from the pK_a values of the electrocatalysts and the pH of the solutions (ranging from 5.25 to 5.55 to match the pH of the systems under CO₂). The rate constant for hydrogen generation, k_{Hy}, was determined over a scan rate less than or equal to 100 mV/s, which was slow enough for the simulation software to detect the coupled chemical step (reaction 3). The data given in Table 1 were reproducible over multiple independent experiments.

Figure 1 shows a comparison of experimental and simulated CVs for pyridinium reduction. The comparison for 4-*tert*-butylpyridinium can be found in the Supporting Information. To assess the accuracy of the data-fitting protocol, the k_{Hy} of pyridinium was also determined using the method described by Olmstead and Nicholson for obtaining the rate constant of a coupled electrocatalytic bimolecular reaction of the same form as reactions 2 and 3.[29] The relation of the ratio of the cathodic and anodic voltammetric waves yielded a k_{Hy} for pyridinium-catalyzed hydrogen generation of 2.7 ± 0.7 M^{-1} s^{-1}, which compares very well to the value reported in Table 1 (see Supporting Information).

It has been observed for a variety of pyridinium analogues that the rate constants, k_{et}, of the charge-transfer reaction can change over an order of magnitude depending on the substituents added to the pyridine ring. The rate of the reaction, as well as the standard potential of reduction, is observed to inversely correlate to the pK_a of the electrocatalyst. Changes in the solution pH over the range of pH 3−6 did not change the observed rate of reaction. This suggests that the increased electron-donating ability of the *tert*-butyl group makes the reduction of the molecule more energy-intensive and the charge transfer slower.

Although only data utilizing platinum electrodes are presented here, there is clearly a critical surface interaction associated with the reduction of pyridinium, since it is observed that the reduction does not occur at all electrode surfaces. For instance, no discernible current is observed by cyclic voltammetry when a glassy carbon electrode is utilized as the working electrode,
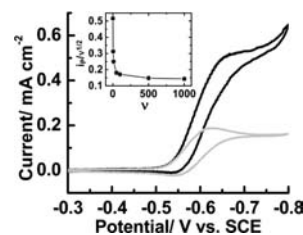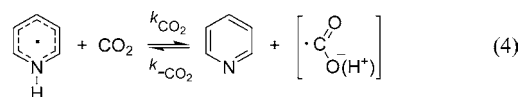
(29) Olmstead, M. L.; Nicholson, R. S. *Anal. Chem.* **1969**, *41*, 862−864.

Figure 2. CVs of pyridinium reduction in the presence of Ar (gray) and CO₂ (black) at pH 5.3, with 0.5 M KCl, and at a scan rate of 1 mV/s. The inset shows the Nicholson and Shain current function (i.e., peak cathodic current over the square root of scan rate) as a function of scan rate (ν) for the CO₂−pyridinium system, typical of an EC′ mechanism. Same Pt disk electrode as Figure 1.

although certain substituted pyridiniums, 4,4′-bipyridinium for example, can be reduced at a glassy carbon surface. While the nature of the surface is therefore critical to pyridinium redox chemistry, pyridinium, when present by itself, does not yield a cyclic voltammetric response that indicates significant chemisorption is associated with its reduction.

Initial CO₂ Reduction by the Pyridinium Radical. Figure 2 shows that, in the presence of CO₂, the cyclic voltammetric cathodic peak current associated with pyridinium reduction is enhanced, which is characteristic of a catalytic interaction. Analysis of CVs obtained at various scan rates using Nicholson−Shain diagnostics confirms an EC′-type mechanism.[30,31] The inset of Figure 2 shows the current-function relation to scan rate consistent with this EC′ mechanism. Other diagnostic criteria are available in the Supporting Information. A direct CO₂ reduction wave was also observed at Pt (see Supporting Information). However, bulk electrolysis at this potential in the absence of pyridinium did not lead to the production of any observed products. Analysis to date of experimental CVs suggests that this direct CO₂ reduction process runs in parallel with the pyridinium-catalyzed process and is not coupled to it. We continue to study this direct process and will report more thoroughly on it in the future.

A likely source for the high activation energy that is typically necessary to reduce CO₂ is the change in orbital hybridization and geometry the molecule experiences upon addition of the first electron.[32] The one-electron reduction product is thought to be either the radical anion, •CO₂⁻, or the radical hydroxyformyl species, •COOH. In aqueous solution, it is generally thought to be in the solvated hydroxyformyl radical form, though there are discrepancies in the literature regarding the pK_a of this species.[32] Therefore, it is shown in the equations below in a general form.
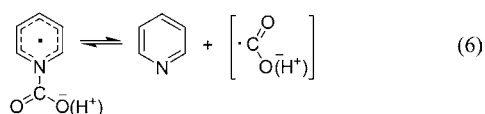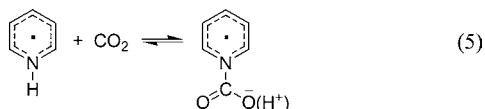
It then follows that a key question is whether the first electron transfer from the pyridinium radical to CO₂ occurs by a simple outer-sphere mechanism to yield this one-electron-reduced product, as depicted in eq 4,

$$\text{(pyridinium radical)} + CO_2 \underset{k_{-CO_2}}{\overset{k_{CO_2}}{\rightleftharpoons}} \text{(pyridine)} + \left[\begin{array}{c} \cdot C \diagup^{O}_{O(H^+)} \end{array} \right] \quad (4)$$

or whether there is evidence for an inner-sphere interaction between the catalyst and substrate involving the formation of a radical pyridinium−CO₂ complex intermediate, as depicted in eqs 5 and 6.

(30) Bard, A. J.; Faulkner, L. R. *Electrochemical Methods, Fundamentals and Applications*, 2nd ed.; Wiley: New York, 2001; pp 501−503.

$$\underset{\overset{|}{N}}{\overset{\cdot}{\bigcirc}} + CO_2 \rightleftharpoons \underset{\overset{|}{\underset{O^{\nearrow}C^{\diagdown}\bar{O}(H^+)}{N}}}{\overset{\cdot}{\bigcirc}} \qquad (5)$$

$$\underset{\overset{|}{\underset{O=C-\bar{O}(H^+)}{N}}}{\overset{\cdot}{\bigcirc}} \rightleftharpoons \underset{N}{\bigcirc} + \left[\overset{O}{\underset{\bar{O}(H^+)}{\cdot C}} \right] \qquad (6)$$

A series of Gaussian 03[33] calculations were performed using the PCM solvation model for water in order to investigate the reaction of the CO_2 with the pyridinium radical. A strong interaction has been found between the pyridinium radical and CO_2, resulting in a predicted N−C bond length of 139 pm and an O−C−O bond angle of 124°, indicating a change in hybridization for the carbon of CO_2 from sp to nearly sp^2, as can be seen in Table 2. The singly occupied HOMO of the pyridine radical−CO_2 complex shows a bonding interaction between the nitrogen of pyridine and the carbon of CO_2 (Figure 3). Interestingly, this nontraditional N−C bond is primarily π-bonding in nature instead of the typical σ bond. The calculated interaction is supported by a gas-phase photoelectron spectroscopy study that reported a pyridine−CO_2^- adduct as a stable species.[34]

Table 3 lists the calculated free energy changes for key conversions in this mechanism using free energies obtained from the Gaussian calculations.[35] It is found that the overall reaction mechanism leading to the production of methanol is energetically favorable. With this computational information, we sought to experimentally confirm whether the interaction between CO_2 and the pyridinium radical goes by either an inner-sphere or an outer-sphere mechanism. To achieve this, the experimentally derived rate constant of the electron transfer from the pyridinium radical to CO_2, k_{CO_2}, and the standard free energy of reaction 4 were related by applying the Marcus cross-relation in eq 7,[36,37]

$$\log k_{CO_2} = \frac{1}{2}\left(\log(k_{cat}k_\sigma f) - \frac{RT}{nF}(E^\circ_{cat} - E^\circ_{CO_2})\right) \qquad (7)$$

where k_{cat} is the self-exchange rate constant for the pyridinium/pyridinium radical redox couple, k_σ is the self-exchange rate constant for the $CO_2/CO_2^\bullet$ redox couple, n is the number of electrons, F is Faraday's constant, f is the Marcus frequency factor, $E^\circ_{CO_2}$ is the standard potential for the reduction of CO_2 (−2.21 V vs SCE), and E°_{cat} is the standard redox potential for the various pyridinium catalysts. In addition to pyridinium and 4-*tert*-butylpyridinium, 2-methylpyridinium and 4-methylpyridinium were also examined. The value for $E^\circ_{CO_2}$ was derived from the redox potential for the reduction of aqueous CO_2 to the solvated hydroxyformyl radical intermediate at our solution

(31) Nicholson, R. S.; Shain, I. *Anal. Chem.* **1964**, *36*, 706–723.
(32) Frese, J. K. W. Electrochemical Reduction of CO_2 at Solid Electrodes. In *Electrochemical and Electrocatalytic Reactions of Carbon Dioxide*; Sullivan, B. P., Krist, K., Guard, H. E., Eds.; Elsevier: Amsterdam, 1993; p 146.
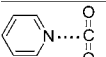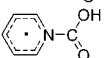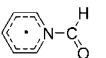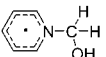(33) Gaussian 03, version C.02; Gaussian, Inc.: Wallingford, CT, 2004.
(34) Han, S. Y.; Chu, I.; Kim, J. H.; Song, J. K.; Kim, S. K. *J. Chem. Phys.* **2000**, *113*, 596–601.
(35) Ochterski, J. W. *Thermochemistry in Gaussian*; Gaussian, Inc.: Wallingford, CT, 2000; pp 1−19.
(36) Gennaro, A.; Isse, A. A.; Saveant, J. M.; Severin, M. G.; Vianello, E. *J. Am. Chem. Soc.* **1996**, *118*, 7190–7196.
(37) Rudolph, M.; Dautz, S.; Jager, E. G. *J. Am. Chem. Soc.* **2000**, *122*, 10821–10830.

Table 2. Structural Parameters for the Various Species Associated with the Reduction of CO_2 to Methanol, Calculated Using the B3LYP/6-31G(D,P) Basis Set

Species	N-C (pm)	C-O (pm)	< N-C-O (deg.)	< O-C-O (deg.)
(pyridine N····C(=O)O)	278[a]	117[a]	92.2[a]	176[a]
(N-C with OH and O)	139	123	124	124
		135	112	
(N-C(H)(=O))	138	123	124	—
(N-C(H)-OH)	143	142	109	—

[a] These values represent a gas-phase calculation using the B3LYP/6-31G(D,P) basis set with no solvation model. Using the PCM model for water to calculate the carbamate zwitterion, a flat potential energy surface was obtained with regard to N−C bond length in the complex.
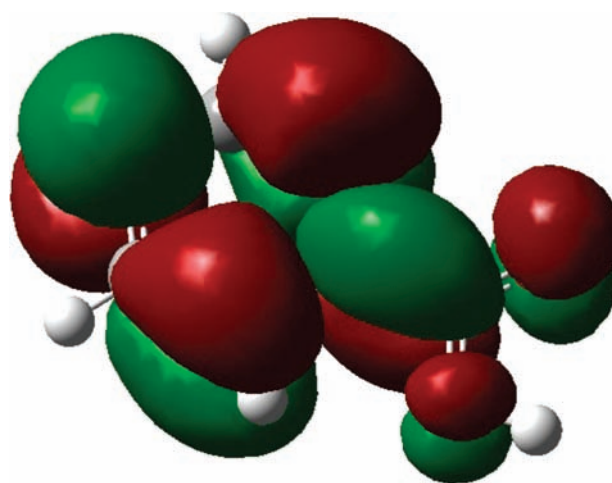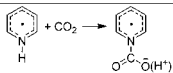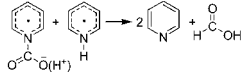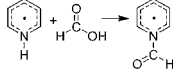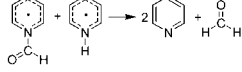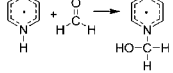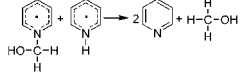

Figure 3. Highest occupied molecular orbital (HOMO) of the pyridinium−CO_2 radical adduct. The HOMO shows a π-bonding interaction between the nitrogen of pyridine and the carbon of CO_2.

pH.[38] The rate constants of reaction 4 for the charge-transfer reaction of the pyridinium radical and CO_2, k_{CO_2}, for the various electrocatalysts were determined by fitting experimental CVs according to reactions 1−4. Figure 4 shows a comparison of the experimental and simulated CVs for the reduction of pyridinium in the presence of CO_2. Similarly good simulated fits were obtained for 4-*tert*-butylpyridinium (Supporting Information) and the methyl-substituted pyridiniums.

Table 4 lists the values for k_{CO_2} for pyridinium and 4-*tert*-butylpyridinium as determined from the digital simulations of the experimental cyclic voltammograms. The variation of k_{CO_2} with the standard free energy of reaction 4 can then be related by plotting $\log k_{CO_2}$ vs ΔE for each catalyst, as given in Figure 5.[36,37] As described by the Marcus cross-relation, the slope of the plot for a simple outer-sphere one-electron-transfer reaction should correlate to 1/120 mV, since the rate constant for a one-electron process is expected to change by 1 order of magnitude when the standard potential varies by 120 mV ($RT/2nF$ at room temperature with $n = 1$). Deviation from the expected 1/120

(38) Frese, J. K. W. Electrochemical Reduction of CO_2 at Solid Electrodes. In *Electrochemical and Electrocatalytic Reactions of Carbon Dioxide*; Sullivan, B. P., Krist, K., Guard, H. E., Eds.; Elsevier: Amsterdam, 1993; p 148.

Table 3. Free Energies of Reactions of Interest in the Reduction of CO_2 to Methanol, Calculated Using Free Energies Obtained for the B3LYP/6-31G(D,P) Basis Set

Rxn Step	Reaction	ΔG kcal mol⁻¹
5		7.46
12		-50.2
16		0.292
17		-38.4
21		1.29
22		-62.5

mV slope means that an inner-sphere mechanism following reactions 5 and 6 could be favored. A slope of 1/55 mV was observed for our series of pyridinium-based catalysts. Following the arguments of previous authors, it is concluded that the observed slope points to an inner-sphere mechanism of reactions 5 and 6. Interestingly, previous application of this mathematical treatment for the catalyzed reduction of CO_2 examined the anion radicals of aromatic nitriles similar to the pyridinium radical catalysts described here.[36]
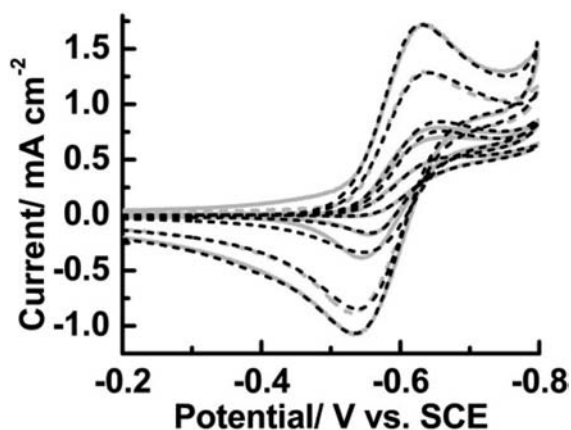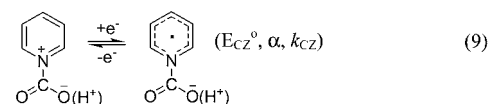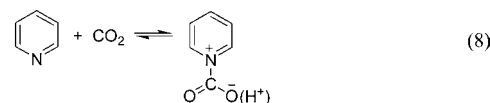
Figure 4. Comparison of experimental (solid) and simulated (dash) CVs for the reduction of pyridinium in CO_2-saturated aqueous solution at pH 5.3 with 0.5 M KCl as supporting electrolyte. Scan rates of 1, 5, 10, 50, and 100 mV/s are shown. Same Pt disk electrode as Figure 1.

Table 4. Kinetic Rate Constants for Electron-Transfer Steps Involving Pyridinium-Catalyzed Reduction of CO_2 en Route to Formic Acid, Formaldehyde, and Methanol

electrocatalyst	$k_{CO_2}{}^a$ (M⁻¹ s⁻¹)	$k_{CHO}{}^b$ (M⁻¹ s⁻¹)	$k_{CH_2O}{}^c$ (M⁻¹ s⁻¹)
pyridinium	1.4	8.9	23
4-*tert*-butylpyridinium	5.7	11	59

a Reaction 4, the reaction of the pyridinium radical with CO_2 yielding the hydroxyformyl radical. *b* Reaction 15, the reaction of the pyridinium radical with the formyl radical yielding formaldehyde. *c* Reaction 21, the reaction of the pyridinium radical with formaldehyde yielding an intermediate species en route to methanol.
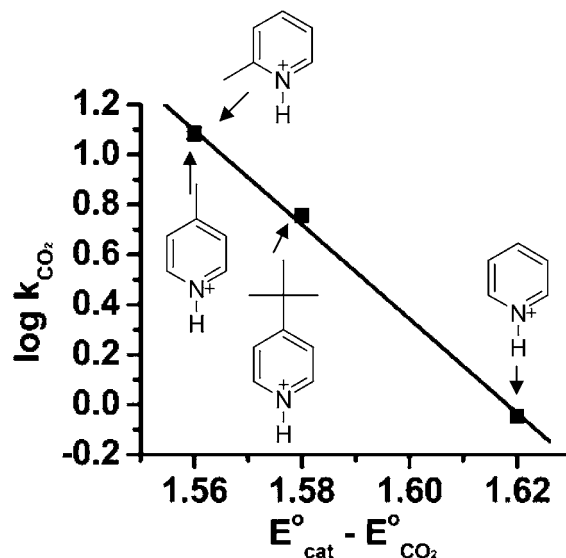
Figure 5. Variation of the rate constant k_{CO_2} with the standard free energy of reaction 4 for pyridinium, 2-methylpyridinium, 4-methylpyridinium, and 4-*tert*-butylpyridinium. The standard potentials for 2-methylpyridinium and 4-methylpyridinium were both −0.64 V vs SCE, as determined by the fitting procedure used for the other electrocatalysts reported in Table 1. The rate constants k_{CO_2} for 2-methylpyridinium and 4-methylpyridinium were 13 and 14 M⁻¹ s⁻¹, respectively, determined using the same fitting procedure for pyridinium and 4-*tert*-butylpyridinium.

On the basis of the computational and experimental evidence for the interaction between CO_2 and the pyridinium radical, the first electron-transfer step appears to proceed through the inner-sphere reaction rather than through a simple outer-sphere mechanism. In fact, satisfactory simulated CVs could also be achieved assuming reactions 5 and 6 instead of reaction 4, and gave similar values. However, another route to the pyridinium radical−CO_2 adduct was also investigated by examining the possibility of pyridine reaction with CO_2 to form a carbamic zwitterion, as depicted in reaction 8. Once formed, this species could be directly reduced by reaction 8 to yield the same pyridinium radical−CO_2 complex given in eq 5.

$$ \text{(pyridine)} + CO_2 \rightleftharpoons \text{(zwitterion)} \qquad (8) $$

$$ \text{(zwitterion)} \underset{-e^-}{\overset{+e^-}{\rightleftharpoons}} \text{(radical)} \quad (E_{CZ}^{\circ}, \alpha, k_{CZ}) \qquad (9) $$

The interaction between pyridine/pyridinium was examined using isotopically enriched $^{13}CO_2$ and ^{15}N pyridine using ^{13}C NMR spectroscopy to probe the existence of a carbamic zwitterion-type species. At a pH of 5.2, a peak associated with dissolved $^{13}CO_2$ can be observed in Figure 6 at approximately 124.6 ppm (slight variations in ppm were seen for small variations in pH). Upon the addition of ^{15}N pyridine, maintaining the same pH of 5.2, a doublet with a 0.48 Hz coupling constant became apparent where the singlet $^{13}CO_2$ was previously observed. The literature reports that $^{15}N-^{13}C$ coupling ranges from 4 to 12 Hz for a well-defined N−C bond. The value observed here therefore suggests a weak interaction between
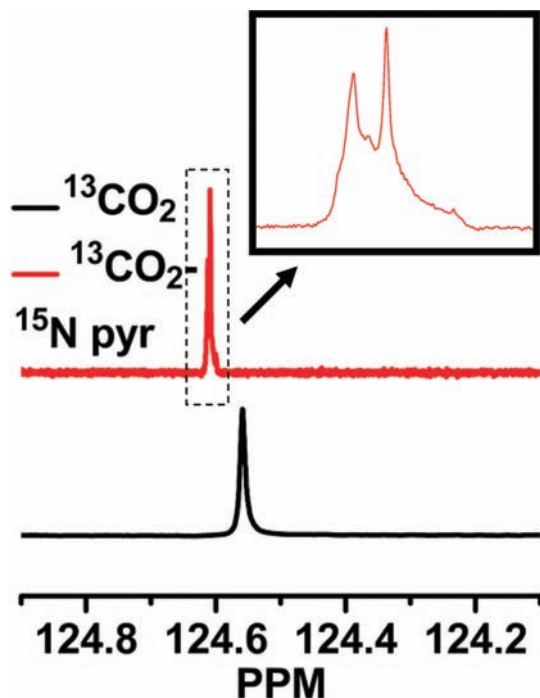
Figure 6. ^{13}C spectra of an aqueous solution containing 10% D_2O, 0.5 M KCl, and 33 mM ^{13}C-enriched $NaHCO_3$, pH adjusted to 5.2 to ensure nearly 100% in the dissolved CO_2 phase (black), with 50 mM ^{15}N-enriched pyridine added (red), maintaining the same pH. Slight discrepancies in the CO_2 peak position are attributed to minor differences in pH. The inset shows an expanded view of the ^{13}C–^{15}N coupling observed between CO_2 and pyridine.

pyridine and CO_2.[39,40] Simple scaling of the observed coupling value argues for a N–C interaction that is approximately 10% of that associated with a N–C single bond. A Gaussian study of the pyridine–CO_2 Lewis acid–base complex also indicates a weak interaction between pyridine and CO_2 with an N–C bond length of 277.6 pm and O–C–O bond angle of 175.6° (Table 2). Applying the Pauling correlation, which relates bond angle to percentage π character of a hybridized orbital, the Gaussian results for the zwitterion species suggest that the CO_2 molecule in the complex is only 10% sp^2 hybridized, retaining 90% of its sp character.

Though this weak interaction was determined to be present, the experimental CVs could not be satisfactorily fit according to reactions 8 and 9 instead of the pyridinium radical-catalyzed mechanism involving reactions 4 or 5 and 6. However, the pyridinium derivative, 4-hydroxypyridinium, did give electrochemical evidence for a small concentration of this species being present in solution, which is directly reducible according to reaction 9. Under Ar, a very small voltammetric response corresponding to the reduction of 4-hydroxypyridinium at pH 4.7 (maintaining the pH observed under CO_2) was observed. At this pH, roughly 0.35 mM of a 10 mM concentration of 4-hydroxypyridine should be in the electroactive 4-hydroxypyridinium form. However, upon bubbling CO_2 while maintaining the same pH, a wave was observed following a CE (a chemical step which generates the electro-active species for a following electrochemical step)-type mechanism, shown in Figure 7.

(39) Bundgaard, T.; Jakobsen, H. J.; Rahkamaa, E. J. *J. Magn. Reson.* **1975**, *19*, 345–356.
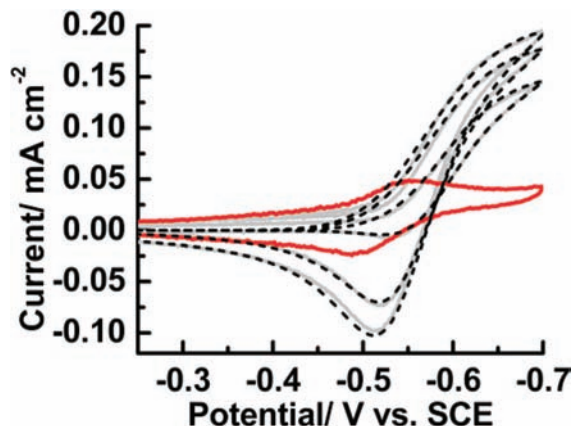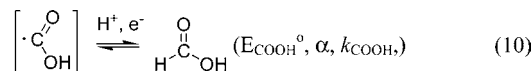(40) Lichter, R. L.; Roberts, J. D. *J. Am. Chem. Soc.* **1971**, *93*, 5218–5224.

Figure 7. Experimental (gray) and simulated (dash) CVs for a CO_2-saturated aqueous solution containing 10 mM 4-hydroxypyridine and 0.5 M KCl at scan rates of 5, 10, and 50 mV/s. The red line represents the same solution purged with Ar, maintained at the same pH. Same Pt disk electrode as Figure 1.

The experimental CVs in Figure 7 could be simulated very well assuming reaction 8 followed by the coupled electrochemical and chemical steps shown in reactions 9 and 6. The average values obtained for the electrochemical parameters in reaction 9 were $E°_{CZ} = -0.38$ V vs SCE and $k_{CZ} = 0.10$ cm/s. The interfacial concentration of the carbamic zwitterion species was only 1.6 μM, as determined by the fitting procedure, and the first-order rate constant for the dissociation of the reduced carbamate species (reaction 6) to yield the hydroxyformyl radical was 0.015 s^{-1}. Therefore, it is reasonable to suggest that a small quantity of a carbamic zwitterion species is present in solution and directly reducible at the electrode. However, it seems that the dominant mechanism for the first electron reduction of CO_2 primarily occurs by reaction with the pyridinium radical, reaction 5.

Once the hydroxyformyl radical is present, a second electron transfer must occur to yield formic acid. Three possible routes were examined. First, it was noticed that, as the CV scan rate was decreased below 10 mV/s, an additional electron-transfer step was required to obtain satisfactory curve-fitting to the experimental CVs. Introduction of reaction 10 provided an excellent fit to the experimental CVs at all scan rates explored.

$$\left[\cdot \overset{O}{\underset{OH}{C}} \right] \overset{H^+, e^-}{\rightleftharpoons} H{-}\overset{O}{\underset{OH}{C}} \quad (E_{COOH}°, \alpha, k_{COOH,}) \qquad (10)$$

Since the experimental CVs were conducted at a Pt electrode, the above reaction correlates well with low hydrogen overpotential metal electrodes where there are ample surface-adsorbed H atoms available to react with a surface species to form formic acid. However, the reaction would be less likely with high hydrogen overpotential materials like p-GaP. Whereas it is reasonable to expect this reaction to take place at Pt and Pd, it is likely that another mechanism dominates in our p-GaP photoelectrochemical system. One possibility is that the production of formic acid could also occur from direct reduction of the pyridinium radical–CO_2 complex from reaction 5, according to eq 11.

$$\qquad (11)$$
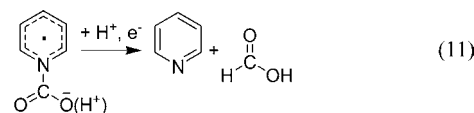
The experimental CVs at Pt could not be simulated to yield satisfactory fits assuming reaction 5 followed by reaction 11. However, molecular orbital calculations suggest it is possible to further reduce the pyridinium radical–CO₂ adduct by an additional charge transfer. Thus, while we rule out this mechanistic path occurring at a Pt electrode, it may be accessible at other interfaces.

Finally, the reaction between the pyridinium–hydroxyformyl radical adduct and another pyridinium radical to produce formic acid and two molecules of pyridine by reaction 12 was also explored.

$$\text{(12)}$$
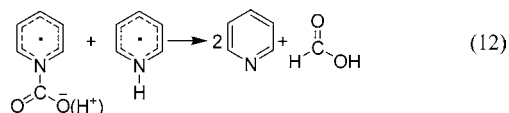
Continuous production of pyridinium radical species at the electrode surface might facilitate such a free radical–free radical reaction. The similar calculated energies (-3.75 eV for the pyridinium radical–CO₂ adduct and -2.75 eV for the pyridinium radical) and orbital symmetries of the π^* HOMOs of the two species suggest the possibility of a $\pi-\pi$ overlap that could facilitate the hypothetical electron transfer of reaction 12.

However, including reaction 12 in the CV digital simulations did not lead to stable values of the respective rate constant for the reaction and did not give satisfactory simulated fits to the experimental curves. Such negative evidence does not definitively rule out the existence of reactions 11 and 12, except at a Pt interface. In Table 3 it is shown that reaction 12 is energetically favorable. We will return to the potential relevance of these reactions with regard to the p-GaP system in a following section. Overall, the mechanistic details shown thus far explain the formation of the two-electron reduction product of carbon dioxide. The carbon of the carbon dioxide functions as an electrophile, as a consequence of the electron-withdrawing nature of the doubly bonded oxygens. The central role of pyridinium radical appears to be that it undergoes a nucleophilic addition–elimination reaction to provide a pyridine-stabilized hydroxyformyl radical.

Reduction of Formic Acid to Formaldehyde by the Pyridinium Radical. The observation of formic acid (pK_a 3.74, primarily formate at the pH of our bulk electrolyses) as an electrolysis product suggested that the reduction of CO₂ leads first to formic acid, followed by the reduction of formic acid to formaldehyde, another observed product. At the bulk pH of the system under evaluation, pH 5.3, formic acid is expected to be mainly present as the formate anion. This species, both in the absence and in the presence of pyridinium, was found to be electrochemically inert under the electrolyte conditions explored. Bulk electrolysis of a solution containing 100 mM formic acid and 10 mM pyridine under Ar adjusted to pH 5.3 ($\sim$100 mM formate, no formic acid) led to no production of methanol.

As the pH of the solution was lowered, allowing the generation of an equilibrium quantity of formic acid, a voltammetric response was observed, corresponding to formic acid reduction. Bulk electrolysis at pH 4.75 containing 33 mM formic acid and 10 mM pyridine led to the production of methanol. A corresponding electrolysis of a formic acid solution at pH 4.75 with no added pyridinium electrocatalyst did not produce methanol or any quantifiable products. Thus, it is concluded that formic acid reduction to methanol is catalyzed by the pyridinium radical and that the reducible species is formic acid rather than formate.

Of course, at the bulk solution pH of the pyridinium–CO₂ cell, there should be practically no quantity of formic acid present. However, the local interfacial pH in our system could potentially differ from the pH of the bulk. To probe the theory of a localized acidic pH gradient near the vicinity of the electrode, bulk electrolysis of our standard CO₂-saturated system containing 10 mM pyridine in addition to 100 mM formic acid was conducted, correcting the bulk pH to the standard 5.3 and operating under our normal galvanostatic conditions of 50 μA cm^{-2}. Thus, in the bulk solution all formic acid should be in the formate form, but if there was an acidic pH gradient near the electrode surface, there could be a quantity of formic acid capable of being reduced. The faradaic efficiency for methanol formation was compared to the faradaic efficiency of the normal CO₂-saturated pyridine system under the same conditions for the electrolysis (i.e., no formic acid added). The faradaic efficiency for methanol was observed to increase from 32% for the CO₂-only system compared to 81% for the CO₂ + formic acid system. Therefore, it can be inferred that the localized pH near the surface of the electrode allows for concentration of formic acid and that pyridinium specifically catalyzes the reduction of formic acid to methanol.

The nature of the interaction of the pyridinium radical with formic acid was examined by simulated CV analysis and computational methods. Formic acid is known to adsorb dissociatively at Pt electrodes to either adsorbed CO[41-46] or formate.[47,48] Here, adsorbed formic acid is assumed to go through the formate intermediate for reasons that correspond to the overall mechanism discussed below in further detail. Dissociative adsorption to adsorbed formate can then be coupled to a 1e$^-$ reduction to the formyl radical, en route to formaldehyde and methanol, as shown in eqs 13 and 14. In fact, the reduction of CO₂ at Pt electrodes is known to yield the strongly adsorbed formyl radical, causing rapid poisoning.[49] The hydroxyformyl radical in eqs 13 and 14 is represented as bonding through the carbon atom for simplicity, though others have proposed formate adsorption through both oxygen atoms as well.[48]

$$\text{(13)}$$

$$\text{(14)}$$
$$(E_{FA}^\circ, \ \alpha, \ k_{FA},)$$
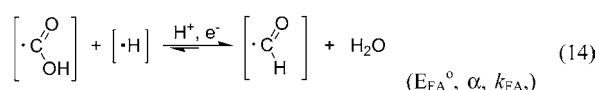
The earlier presence of the surface-adsorbed hydroxyformyl radical that was proposed in eq 9 for the second electron-transfer step is supported by the reappearance of the species in reactions 13 and 14. However, it should be mentioned that while reactions 13 and 14 are plausible at Pt, the presence of adsorbed hydrogen atoms at p-GaP is less likely. Alternate routes are discussed below for this interface. It would then follow that this hydroxyformyl radical at Pt can either be reduced to formic acid, as

(41) Beden, B.; Bewick, A.; Lamy, C. *J. Electroanal. Chem.* **1983**, *148*, 147–160.
(42) Chang, S. C.; Ho, Y. H.; Weaver, M. J. *Surf. Sci.* **1992**, *265*, 81–94.
(43) Iwasita, T.; Nart, F. C.; Lopez, B.; Vielstich, W. *Electrochim. Acta* **1992**, *37*, 2361–2367.
(44) Kunimatsu, K.; Kita, H. *J. Electroanal. Chem.* **1987**, *218*, 155–172.
(45) Sun, S. G.; Clavilier, J.; Bewick, A. *J. Electroanal. Chem.* **1988**, *240*, 147–159.
(46) Sun, S. G.; Lin, Y.; Li, N. H.; Mu, J. Q. *J. Electroanal. Chem.* **1994**, *370*, 273–280.
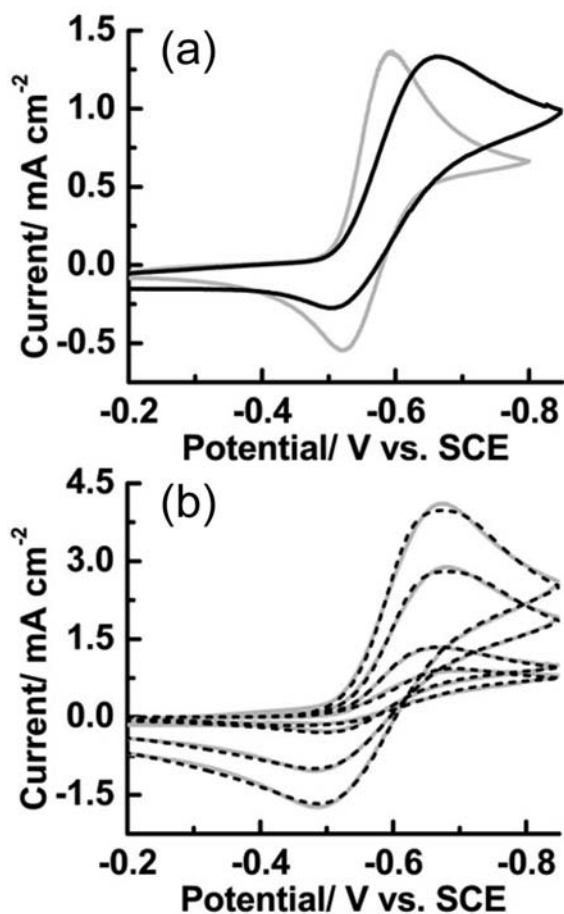
Figure 8. (a) CVs of formic acid reduction (gray) and in the presence of 10 mM pyridine (black) at pH 4.75 to yield 20 mM formic acid in solution, with 0.5 M KCl at a scan rate of 10 mV/s. (b) Experimental (solid) and simulated (dash) CVs for the solution in (a) at scan rates of 5, 10, 50, and 100 mV/s. Same Pt disk electrode as Figure 1.

depicted by reaction 10, or follow reaction 14 to yield a possible surface-adsorbed formyl radical. This reaction technically corresponds to two electron transfers since it involves an adsorbed hydrogen atom. However, the addition of the proton and electron to yield the formyl radical and water is coupled to reaction with the adsorbed hydrogen atom such that the two processes were not able to be distinguished from each other in the digital simulations. Thus, the reaction is represented as a single electrochemical step with the electrochemical parameters in reaction 14. Experimental CVs for the direct reduction of formic acid at a pH of 4.75 could be fit very well according to reactions 13 and 14 (see Supporting Information). Limited reversibility of the reaction was observed, with multiple CVs producing an increasing peak-to-peak separation and decreasing peak height associated with the poisoning of the electrode from this reduced species. Polishing for ~1 min with 5 μm polishing alumina was required to re-establish electrode activity. For the direct reduction of formic acid, the average values obtained for the electrochemical parameters in reaction 14 were $E^\circ_{FA} = -0.56$ V vs SCE, $k_{FA} = 0.005$ cm/s.

Upon addition of pyridine to the formic-acid-containing solution, the voltammetric response was observed to change, and the CVs became stable over continuous cycling. Figure 8a shows a reduction in the return oxidation wave for formic acid

in the presence of pyridine. This response is consistent with the reaction of the pyridinium radical with a surface formyl radical (reaction 14) to yield formaldehyde. In addition, X-ray photoelectron spectroscopy (XPS) analysis of the electrodes after electrolysis did not show any evidence of poisoning surface species, supporting the reaction of the pyridinium radical with a surface formyl radical (see Supporting Information). To examine this hypothesis, a bulk electrolysis was performed using the same electrochemical parameters as described above for the reduction of formic acid, but employing a Pt rotating disk electrode. The rotating disk produced a controlled mass transport of pyridinium to the electrode surface for reduction to the pyridinium radical but limited the residence time of this species at the electrode–electrolyte interface, thereby minimizing the interaction of this species with the anticipated surface-adsorbed formyl moiety. At a rotation speed of 1000 rpm, only trace levels of methanol were produced, as expected if a pyridinium radical–surface formyl interaction existed. Also, the experimental CVs for the pyridinium and 4-*tert*-butylpyridinium electrocatalysts could be fit satisfactorily following reactions 13 and 14, coupled to the reduction of the formyl radical by the pyridinium radical, as given in reaction 15. The CV derived rate constants for reaction 15 are reported in Table 4.
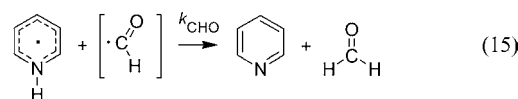

Figure 8b shows a comparison of the experimental and simulated CVs according to the reactions 13–15 for the reaction of the pyridinium radical with formic acid. Comparisons for 4-*tert*-butylpyridinium yielded equally good simulated curves and can be found in the Supporting Information.

Thus far, the electrochemical evidence for the mechanism of formic acid reduction to formaldehyde has been presented. The mechanism was further explored using Gaussian calculations to examine the interaction between the pyridinium radical and formic acid, analogous to the interaction between the pyridinium radical and CO_2, as given by reaction 16.
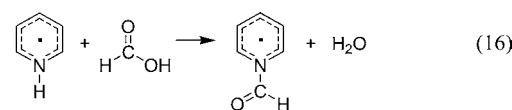
The resulting pyridinium–formyl radical adduct can then react with pyridinium radical, resulting in the formation of formaldehyde and two molecules of pyridine (reaction 17).
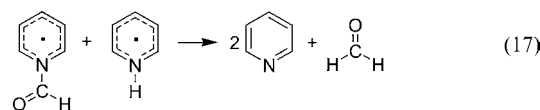
The calculated HOMO of the pyridine–formyl radical adduct shows a bonding interaction between the nitrogen of pyridine and the carbon of the formyl group. The nitrogen–carbon bond

(47) Columbia, M. R.; Crabtree, A. M.; Thiel, P. A. *J. Am. Chem. Soc.* **1992**, *114*, 1231–1237.
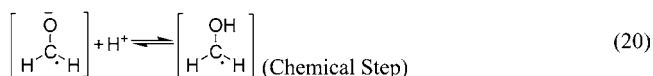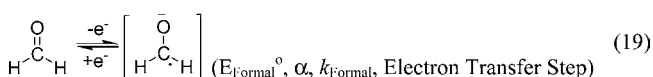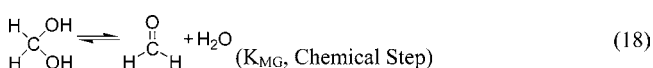(48) Szklarczyk, M.; Sobkowski, J.; Pacocha, J. *J. Electroanal. Chem.* **1986**, *215*, 307–316.
(49) Halmann, M. M.; Steinberg, M. Electrochemical Reduction of CO_2. In *Greenhouse Gas Carbon Dioxide Mitigation: Science and Technology*; Halmann, M. M., Steinberg, M., Eds.; Lewis Publishers: Boca Raton, FL, 1999; p 415.

length and the N−C−O bond angle are given in Table 2 and indicate a rehybridization of the CO_2 to sp^2. The HOMO of the pyridine−formyl radical adduct and the HOMO of the pyridinium radical can overlap in a π-fashion to facilitate charge transfer. However, high-quality simulations of the experimental CVs could not be attained over a range of electrocatalysts utilizing the reactions given in eqs 16 and 17. The reduction of formic acid by the pyridinium radical to formaldehyde is the least energetically favorable of the three coupled two-electron steps, −38 kcal/mol. The transfer of the first two electrons to yield formic acid is −43 kcal/mol, and the transfer of the last two electrons to formaldehyde to yield methanol is −61 kcal/mol. This correlates to the fact that formic acid is observed as a reaction product and is not completely converted to formaldehyde and ultimately methanol.

Formaldehyde Reduction to Methanol by the Pyridinium Radical. We have previously reported the formation of trace levels of formaldehyde during the reduction of CO_2 in our pyridinium-catalyzed system at Pd electrodes.[14] However, this earlier work was indeterminate as to whether formaldehyde acted as an intermediate in methanol production. Thus, we focused on determining the route to methanol formation and the possible role of formaldehyde. Formaldehyde itself is known to be electroactive and can be reduced to methanol at certain electrode materials by a $2e^-$ process.[50] Subtle variations of the mechanism have been observed depending on the pH of the solution, though generally the mechanism can be described as CECE (chemical step, followed by an electrochemical step, a second chemical step, and a second electrochemical step).[50] A $1e^-$ wave was observed under acidic conditions (pH 3) for the reduction of formaldehyde at a Pt electrode. Acidic conditions were chosen in line with the data presented for formic acid, which suggests an acidic environment near the electrode interface. In order to obtain a voltammetric response attributable to formaldehyde, CV analyses were carried out using a commercially available 38% formaldehyde solution. Aqueous formaldehyde solutions are primarily in the nonelectroactive hydrated form of formaldehyde, methylene glycol. The equilibrium highly favors the methylene glycol form, leading to <0.1% formaldehyde in aqueous solution.[51]

Importantly, our experimental CVs for the direct reduction of formaldehyde could be simulated very well using the CEC reaction scheme given in eqs 18−20, which is consistent with the CECE mechanism noted above.

$$\begin{matrix} H \\ & C \\ H \end{matrix} \begin{matrix} OH \\ \\ OH \end{matrix} \rightleftharpoons \begin{matrix} & O \\ H & \parallel \\ & C \\ H \end{matrix} + H_2O \quad (K_{MG}, \text{Chemical Step}) \qquad (18)$$

$$\begin{matrix} O \\ \parallel \\ H-C-H \end{matrix} \xrightarrow[+e^-]{-e^-} \left[\begin{matrix} \bar{O} \\ | \\ H-C^{\cdot}-H \end{matrix} \right] (E_{Formal}^{\circ}, \alpha, k_{Formal}, \text{Electron Transfer Step}) \qquad (19)$$

$$\left[\begin{matrix} \bar{O} \\ | \\ H-C^{\cdot}-H \end{matrix} \right] + H^+ \rightleftharpoons \left[\begin{matrix} OH \\ | \\ H-C^{\cdot}-H \end{matrix} \right] (\text{Chemical Step}) \qquad (20)$$

The last electron-transfer step includes a proton-coupled electron transfer to yield methanol and could not be detected satisfactorily by the CV simulation software. This redox reaction was thus omitted in the fitting routine. For the direct reduction of formaldehyde, the average values obtained for the electro-
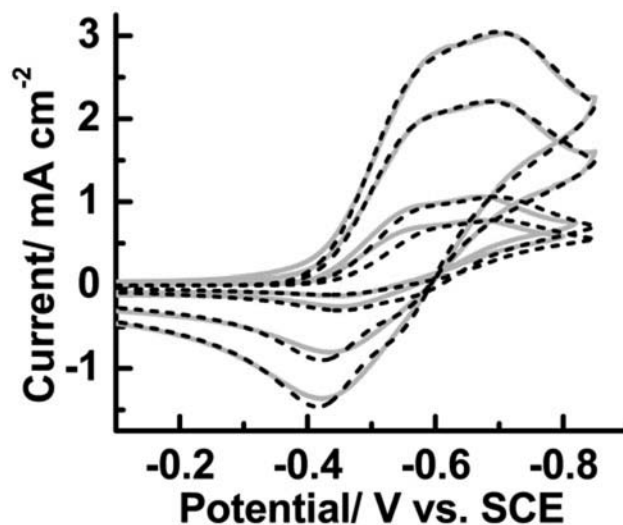
(50) Clarke, S.; Harrison, J. A. *J. Electroanal. Chem.* **1972**, *36*, 109–115.
(51) Bell, R. P.; Evans, P. G. *Proc. R. Soc. London, Ser. A* **1966**, *291*, 297–323.

Figure 9. Experimental (solid) and simulated (dash) CVs for a ~37.25 M aqueous solution of formaldehyde (mostly methylene glycol, <0.1% in formaldehyde form, ~11 mM formaldehyde) containing 0.5 M NaCl and 10 mM pyridine at scan rates of 5, 10, 50, and 100 mV/s. Same Pt disk electrode as in Figure 1.

chemical parameters in reaction 19 were $E^{\circ}_{formald} = -0.50_5$ V vs SCE, $k_{formald} = 0.002$ cm/s.

Importantly, the K_{MG} obtained from the fitting procedure (~8 × 10^{-4}) for eq 18 corresponded very well to the equilibrium constant reported in the literature of ~5 × 10^{-4}.[51] This leads to an expected formaldehyde volume percent of <0.1%. A comparison of the simulated and experimental CVs for formaldehyde alone is given in the Supporting Information. At Pt, repeated CV cycling led to the fouling of the electrode surface. Reproducible CVs were obtained only by polishing the electrode between scans for ~1 min with 5 μm polishing alumina. Upon the addition of 10 mM pyridine, fouling of the electrode was observed. Therefore, it cannot be assumed that the pyridinium radical interacts with any of the surface-adsorbed species present by the direct reduction of formaldehyde. Either the pyridinium radical must react with formaldehyde directly before surface adsorption can proceed, or possible physisorption of pyridinium/pyridine at the electrode surface must effectively block fouling from the direct reduction of formaldehyde.

Following these hypotheses, XPS analysis after the bulk electrolyses did not show any evidence for the fouling or poisoning of the electrodes (see Supporting Information). The steady-state approximated concentration of formaldehyde is assumed to be low due to the comparison of the rate constant for formaldehyde generation, k_{CHO}, to the rate constant for formaldehyde reduction, k_{CH_2O}, given in Table 4. The formaldehyde concentration is also assumed to be much smaller than the concentration of the pyridinium radical generated near the electrode surface. The rate constant k_{et} for the generation of the pyridinium radical reported in Table 1 is 0.010 cm/s, compared to the rate constant for direct reduction of formaldehyde, $k_{formald}$ = 0.002 cm/s. Not only is the rate constant for pyridinium reduction 5 times higher than $k_{formald}$, but the concentration of formaldehyde should be much lower than the pyridinium concentration at the electrode interface, which is ~4.5 mM. Thus, there should be ample quantities of the electrogenerated pyridinium radical near the electrode surface to react with formaldehyde before direct reduction.

Figure 9 shows a comparison of experimental and simulated CVs for the reduction of formaldehyde in the presence of

Scheme 1. Overall Proposed Mechanism for the Pyridinium-Catalyzed Reduction of CO₂ to the Various Products of Formic Acid, Formaldehyde, and Methanol
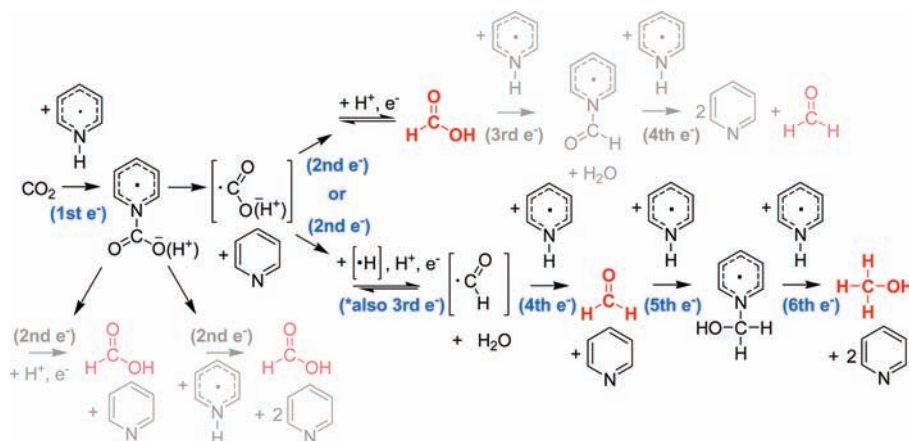

pyridinium at pH 3; the CVs for 4-*tert*-butylpyridinium are given in the Supporting Information. The first wave is attributed to the direct reduction of formaldehyde by reaction 19, and the second reduction wave is assigned to the reduction of pyridinium according to reaction 2.

Very good simulated fits to the experimental CVs could be obtained assuming the reactions of 18–20 along with reaction 21.
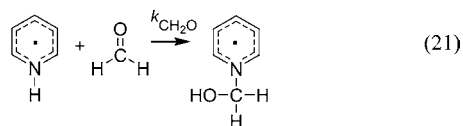

The rate constants for reaction 21 are reported in Table 4. It is assumed that further reaction of the pyridinium–formyl radical complex with another pyridinium radical is a probable route to methanol, as shown in reaction 22.
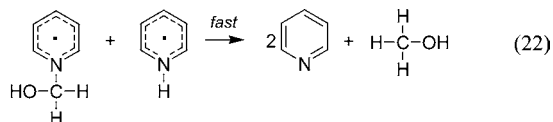
Applying reaction 22 to the fitting routine led to drifting values of the respective second-order rate constant. This instability was traced to a very large rate constant for reaction 22. The proposed mechanistic steps appear valid as long as reaction 22 is fast compared to reaction 21.

Unfortunately, bulk electrolyses, either in the presence or in the absence of pyridinium, could not be carried out for formaldehyde, since stock solutions of formaldehyde contain large quantities of methanol (roughly 15% v:v) as a stabilizer. Likewise, dissolving paraformaldehyde in aqueous solution leads to the production of interfering amounts of methanol and formic acid by the Cannizaro reaction, shown in reaction 23.[52–55]
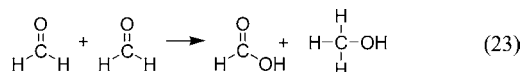
Gaussian calculations, however, suggest that the pyridinium radical can be anticipated to react with formaldehyde in an inner-sphere manner to produce the pyridine–hydroxymethyl radical adduct shown in Table 2, corresponding to reaction 21. This free radical has an N–C bond length and N–C–O bond angle indicating that the carbon of formaldehyde has undergone a

hybridization change from sp² to sp³. Gaussian calculations reveal that the HOMO of pyridine–hydroxymethyl radical adduct constitutes a bonding interaction between the nitrogen and the carbon of hydroxymethyl moiety. Reaction of the pyridine–hydroxymethyl radical adduct with pyridinium radical is then expected to yield methanol, as shown in reaction 22.

The HOMO of the pyridine–hydroxymethyl radical adduct and the HOMO of the pyridinium radical have compatible orbital symmetry for charge-transfer overlap. From the calculated free energy changes for key conversions in this mechanism using energies obtained from Gaussian calculations, the pyridinium-radical-catalyzed reduction of formaldehyde is found to be the most energetically favorable of the series of two-electron steps (Table 3). Similarly, the rate constants for formaldehyde reduction, k_{CH_2O}, for both pyridinium and 4-*tert*-butylpyridinium are the highest in Table 4, consistent with the observation of only trace levels of formaldehyde in our systems.

It was also observed that dissolving paraformaldehyde in aqueous solution at our system pH by heating to ∼65 °C led to the production of methanol and formic acid, following the Cannizaro reaction. This led to the possibility that our observed products of formic acid and methanol could be produced through this chemical reaction instead of by pyridinium-catalyzed electroreduction. However, reducing the pH of our solution to pH 3, where the Cannizaro reaction was not detected, did not affect the faradaic yields for methanol and formic acid, ruling out the presence of a Cannizaro-type mechanism.

Analysis of Reaction Rates and Product Yield. The overall proposed mechanism for the reduction of CO₂ to the various products of formic acid, formaldehyde, and methanol is represented in Scheme 1. The light gray area represents alternate possible routes to formic acid and formaldehyde that could potentially occur but could not be unambiguously identified from the available data at a Pt interface. The main mechanistic route correlates to the observed data presented in the previous sections. Importantly, it seems that the formation of either formic acid or formaldehyde (which is further reduced to methanol) goes through a key intermediate, the hydroxyformyl radical, as outlined in reactions 10 and 14. The direct reduction of this species yields either formic acid or the formyl radical, as seen

(52) Birstein, G.; Lobanow, N. *Z. Anorg. Chem.* **1927**, *160*, 377–386.
(53) Geib, K. H. *Z. Phys. Chem.* **1934**, *169*, 41–51.
(54) Martin, R. J. L. *Aust. J. Chem.* **1954**, *7*, 335–347.
(55) Molt, E. L. *Recl. Trav. Chim. Pays-Bas* **1937**, *56*, 233–246.

Table 5. Results for Bulk Electrolyses[a] at Hydrogenated Pd[b] or Pt Electrodes Galvanostatically Held at 50 μA cm^{-2} for Various Pyridinium Electrocatalysts (10 mM in 50 mL of H₂O + 0.5 M KCl as Supporting Electrolyte Saturated with CO₂)

electrocatalyst[c]	HCOOH[d] faradaic yield (%)	CH₃OH faradaic yield (%)	total yield[e] (%)
pyridinium	10.8 ± 0.5	22 ± 2	33 ± 3
4-*tert*-butylpyridinium	trace	14.5 ± 2	14.5 ± 2

[a] Representing the average over at least three experiments. [b] See Experimental Section for details on hydrogenation. [c] Formaldehyde concentrations seem to be at trace levels. [d] Mostly in the formate form at the pH's of the solutions used. See Experimental Section. [e] Total faradaic yield for observed CO₂-derived products, not including competing hydrogen generation.

in Scheme 1. The formyl radical is then further reduced to methanol through reduction by the pyridinium radical. It should be noted that, at Pt, any formic acid generated can also dissociatively adsorb at the electrode surface, regenerating the hydroxyformyl radical and an adsorbed hydrogen atom that could then be reduced to the formyl radical. This would reduce formic acid concentrations and ultimately increase methanol yields.

We sought to correlate our experimentally obtained faradaic efficiencies for formic acid and methanol to the observed kinetic constants calculated from our fitting procedures. Galvanostatic electrolyses in a CO₂-saturated aqueous electrolyte solution containing 10 mM of the pyridinium-derived electrocatalyst yielded primarily methanol and formic acid, with trace levels of formaldehyde. Similar faradaic efficiencies for the observed products were obtained at both Pt and Pd interfaces. The results of bulk electrolyses for pyridinium and 4-*tert*-butylpyridinium are given in Table 5.

For both pyridinium and 4-*tert*-butylpyridinium, the rate-limiting step appears to be the first electron transfer from the pyridinium radical to CO₂, as reported in Table 4 as the second-order rate constant, k_{CO_2}. This conclusion is supported by the calculated free energies given in Table 3 for the various reaction steps, which confirms that the first electron-transfer step is endoenergetic. In order to determine the three rate constants in Table 4, separate CV experiments had to be performed to examine the pyridinium-catalyzed reduction of either CO₂, formic acid, or formaldehyde alone, as described in the prior sections. Since the first electron-transfer step to CO₂ is rate-limiting for both pyridinium- and 4-*tert*-butylpyridinium-catalyzed CO₂ reduction, a steady-state approximation for the formation of the hydroxyformyl radical is valid, allowing the determination of the relative rates of production of formic acid and methanol through the competing electron-transfer steps, (I) and (II), shown in Scheme 2.

Analysis of the concentration profiles of various reaction species obtained from fitting our experimental CV curves to the simulated curves confirms a steady-state concentration of the hydroxyformyl radical near the vicinity of the electrode for both pyridinium and 4-*tert*-butylpyridinium. Using these steady-state concentrations and the calculated rate constants for competing reactions (I) and (II) in Scheme 2, the rates of formation of formic acid and the intermediate formyl radical could be determined and related to the faradaic yields of the observed products. The comparison of rates of production of formic acid and the formyl radical are given in Table 6, along with the calculated faradaic yields for formic acid and methanol.

The calculated faradaic efficiencies compare very well to the experimentally observed faradaic yields reported in Table 5,

Scheme 2. Branched Mechanism Showing the Important Kinetic Constants Leading to the Competing Formation of Formic Acid and Methanol
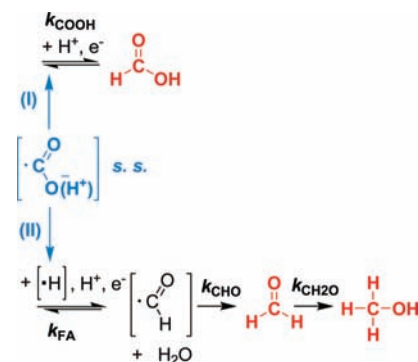
giving further support to the proposed mechanism in Scheme 1. For instance, the smaller k_{COOH} value observed for 4-*tert*-butylpyridinium compared to pyridinium leads to the decreased production of formic acid, which is also seen in the bulk electrolysis experiments in Table 2. The slightly lower calculated faradaic efficiency for formic acid using a pyridinium catalyst compared to experimental values could relate to the other formic acid pathways in Scheme 1 also occurring. It should be mentioned that generally the rate constant, k_{CHO}, should be roughly 10 times higher than the limiting step to apply the steady-state approximation described here. For pyridinium, this factor is approached, but for 4-*tert*-butylpyridinium, $k_{CHO} = \sim 2k_{CO_2}$. However, this concern is lessened by the precise comparison between experimental and calculated faradaic efficiency values.

From the concentration profiles, the steady-state concentration of hydrogen was found to be 1.5×10^{-8} mol cm^{-3}, as generated by reaction 3. Compared to the steady-state concentration of the hydroxyformyl radical given in Table 5, 4×10^{-8} mol cm^{-3}, and adjusted to account for the fact that hydroxyformyl radical formation is a 1e$^-$ process and hydrogen generation is a 2e$^-$ process, the partitioning of electrons between CO₂ reduction and hydrogen production is roughly 58% to 42%. A faradaic yield of 42% for hydrogen generation, coupled to the 33% observed for the reduction of CO₂ to quantifiable products in the presence of pyridinium, gives a total faradaic yield of 75%. When employing low hydrogen overpotential electrode materials such as Pt and Pd for the reduction of CO₂, competing proton reduction to hydrogen is always an issue. It can be inferred, then, that the use of high hydrogen overpotential electrode materials would lead to an increase in faradaic yield for CO₂-derived products and a decrease in hydrogen production. The increased faradaic yields observed at p-GaP, a high hydrogen overpotential material, illustrates this effect. A higher ratio of electrons going to the reduction of CO₂ would lead to increased rates of production for the hydroxyformyl radical and subsequently increased methanol yields. Formic acid was not observed in quantifiable amounts at p-GaP in contrast to Pt and Pd electrodes. This experimental observation is consistent with the formation of formaldehyde via reactions 16 and 17, which were not observed to occur to any appreciable extent at Pt electrodes. However, at high hydrogen overpotential electrode materials, where surface hydrogen atoms are less likely, the reaction could be catalyzed completely through reduction by the pyridinium

Table 6. Comparison of the Rates of Production of Formic Acid and Methanol (through Formaldehyde) from the Two Competing Electron-Transfer Reactions of k_{COOH} (to Formic Acid) and k_{FA} (to Formyl Radical)

electrocatalyst	[•COOH] (mol cm^{-3})	k_{COOH} (cm s^{-1})	k_{FA} (cm s^{-1})	HCOOH rate (mol cm^{-2} s^{-1})	[•CHO] rate (mol cm^{-2} s^{-1})	calculated faradaic yield range HCOOH (%), CH$_3$OH (%)
pyridinium	4×10^{-8}	$2 \times 10^{-4} \pm 1 \times 10^{-4}$	$1.0 \times 10^{-3} \pm 0.2 \times 10^{-3}$	$3.6 \times 10^{-12} \pm 1.8 \times 10^{-12}$	$4.0 \times 10^{-11} \pm 0.8 \times 10^{-11}$	$1._5$–$4._5$, 18–28
4-*tert*-butylpyridinium	$9._5 \times 10^{-9}$	$1.6 \times 10^{-4} \pm 0.7 \times 10^{-4}$	$3.3 \times 10^{-3} \pm 0.9 \times 10^{-3}$	$1.5 \times 10^{-12} \pm 0.6 \times 10^{-12}$	$3.1 \times 10^{-11} \pm 0.9 \times 10^{-11}$	<1, 13–23

radical. The fact that the overall mechanism shown in Table 3 is exoenergetic supports this molecule-only-based mechanism.

Conclusions

Pyridinium-based catalysts are effective and stable catalysts for the reduction of CO_2 to various products operating at low overpotential. Surprisingly, it appears that the pyridinium radical, a one-electron charge-transfer mediator, is capable of efficiently transferring all six electrons necessary for transforming CO_2 to methanol. Furthermore, it appears that the pyridinium radical can react with the various species and intermediates through a coordinative interaction that stabilizes the intermediate species. This simple, organic molecule can thus reduce CO_2 to highly reduced species through multiple electron transfers without the need for a metal-based multielectron transfer. This finding stands in contrast to current thinking that assumes fuel-forming reactions will only be energetically favorable if a multielectron charge-transfer reagent is employed. It is not common that a single catalyst has the ability to reduce multiple species. This observation enhances the novelty of pyridinium as an electron shuttle. This property is also proposed to be the reason that such high faradaic yields can be obtained at both metal and semiconductor electrode materials. That is, while there are clearly surface-sensitive aspects to the described chemistry, the mechanism in many respects either is dominated by solution processes or is sufficiently branched that, in the absence of an electrocatalytic interface, an alternate homogeneous reaction pathway of similar energy is available. The nature of the described reactivity is such that, while one expects low-energy dynamics at a variety of electrode interfaces, the ratio of products observed and the overall faradaic efficiency to a specific product are expected to be strongly electrode dependent.

Experimental Section

Chemicals and Materials. All pyridines were >98% purity and used as received without further purification (Aldrich). Either deionized or high-purity water (Nanopure, Barnstead) was used to prepare the aqueous electrolyte solutions. The electrochemical system was composed of a standard two-compartment electrolysis cell to separate the anode and cathode reactions containing 0.5 M KCl (EMD > 99%) as supporting electrolyte and 10 mM of the desired pyridine. The working electrode consisted of a known area Pt foil connected to a Pt wire (both Aldrich) or a Pd foil (Johnson Matthey). Pd electrodes were hydrogenated at a current density of 15 mA cm^{-2} in 1 M H$_2$SO$_4$ until ~73 C passed. All potentials stated were referenced against a saturated calomel electrode (Accumet). The three-electrode assembly was completed with a Pt mesh electrode also connected to a Pt wire. Before and during all electrolyses, CO$_2$ (Airgas) was continuously bubbled through the electrolyte to saturate the solution. The resulting pH of the solution was maintained at pH 4.7–5.6, depending on the substituted pyridine employed. Under constant CO$_2$ bubbling, the pH values of 10 mM solutions of 4-hydroxypyridine, pyridine, and 4-*tert*-butylpyridine were 4.7, 5.28, and 5.55, respectively. For NMR experiments, isotopically enriched [^{15}N]pyridine (>98%) and [^{13}C]-NaHCO$_3$ (99%) were obtained from Cambridge Isotope Laboratories, Inc.

Cyclic Voltammetry and Bulk Electrolyses. Bulk electrolysis experiments were performed using a PAR 173 potentiostat–galvanostat together with a PAR 379 digital coulometer (three-electrode assembly) or a LakeShore current source (two-electrode assembly omitting the reference electrode). Bulk electrolyses were run under galvanostatic conditions, unless otherwise noted, at 50 μA cm^{-2} for 24–30 h. CVs were obtained using a PAR 273 potentiostat–galvanostat or a DLK-60 electrochemical analyzer at scan rates ranging from 0.5 to 1000 mV/s at a Pt disk electrode (0.1257 cm^2). The pH values of the solutions were always maintained at the pH observed under CO$_2$ bubbling and were adjusted with 1 M H$_2$SO$_4$ under Ar.

Gas Chromatography. The electrolysis samples were analyzed using a gas chromatograph equipped with an FID detector for the presence of methanol and other volatile organics. Removal of the supporting electrolyte salt was first achieved with Amberlite IRN-150 ion-exchange resin (cleaned prior to use to ensure no organic artifacts by stirring in a 0.1% v/v aqueous solution of Triton X-100 reduced (Aldrich), filtered, rinsed with a copious amount of water, and vacuum-dried below the maximum temperature of the resin) before the sample was directly injected into an HP 5890 GC which housed a DB-Wax column (Agilent Technologies). The injector temperature was held at 200 °C, the oven temperature at 120 °C, and the detector temperature at 200 °C.

NMR. NMR spectra of electrolyte volumes after bulk electrolyses were also obtained using an automated Bruker Ultrashield 500 Plus spectrometer with an excitation sculpting pulse technique for water suppression.[56] Data processing was achieved using MestReNova software. The concentrations of formate and methanol present after bulk electrolyses were determined using acetone as the internal standard. For ^{15}N–^{13}C coupling experiments, ^{13}C NMR spectra were obtaining using an automated Bruker Ultrashield 500 Plus spectrometer tuned for maximum ^{13}C sensitivity. In a typical experiment, an aqueous solution containing 10% deuterium oxide (Cambridge Isotope Laboratories, Inc., >99.9%), 0.5 M KCl, 50 mM [^{15}N]pyridine, and 33 mM [^{13}C]NaHCO$_3$ was first purged with Ar in a septa-sealed NMR tube, and then the pH was adjusted using 1 M H$_2$SO$_4$ to a pH of 5.2. At this pH the bicarbonate was observed to be completely in the dissolved ^{13}CO$_2$ form. No peak associated with H^{13}CO$_3$ was seen. The temperature of the experiment was maintained at 295 K; however, the temperature of the instrument was also adjusted to assess the temperature dependence on the ^{15}N–^{13}C coupling. The sample tube was held for at least 10 min at the given temperature before the spectra were obtained to ensure temperature equilibrium. A temperature range of 275–306 K was examined.

CV Simulations. Simulations of experimental CVs were generated using the DigiElch 4.0 simulation software and the fitting routines and reactions described in the text. Diffusion coefficients for all species were estimated at 1×10^{-5} cm/s. As discussed, the fitting routine was allowed to determine the concentration of the pyridinium form present in solution. Overall, the program determined a concentration similar to that predicted by the pH of the solution. The concentration of CO$_2$ was set at 33 mM. $E°$, α, and k_s for all electron-transfer steps were allowed to be determined by the fitting software, as well as the k_s values for all chemical reactions. The scan rate for each experimental CV and electrode area (0.1257 cm^2) were imported.

(56) Hwang, T.; Shaka, A. *J. Magn. Reson., Ser. A* **1995**, *112*, 275–279.

XPS. X-ray photoelectron spectra were collected using a VG Scientific ESCALAB2 spectrometer with monochromated Mg Kα radiation ($h\nu$ = 1253.6 eV). Emitted photoelectrons were detected by a hemispherical analyzer. Operating pressure in the sampling chamber was below 1×10^{-8} Torr. A pass energy of 20 eV was used for high-resolution measurements of C 1s, O 1s, N 1s, Pt 4f, and Pd 3d regions. For all measurements the binding energy scale was normalized to the position of the C 1s peak. Curve-fitting of the core-level XPS lines was carried out by CASA XPS software with a Gaussian–Lorentzian product function and nonlinear Shirley[57] background subtraction. Pt reference samples were prepared by first cleaning in concentrated HNO₃, followed by through rinsing with deionized water and subsequent flame-annealing. Pd reference samples were dipped briefly in concentrated HNO₃ before hydrogenation as described above. X-ray photoelectron spectra were obtained for both Pt and hydrogenated Pd after bulk electrolyses either in the presence or in the absence of CO₂, held galvanostatically at 50 μA cm^{-2} for 24 h in the same 10 mM pyridine solution with 0.5 M KCl as described above. After the bulk electrolyses were ended, the samples were removed from the solution, rinsed with deionized water, and air-dried before being immediately placed in the sampling chamber.

Computational Methods. All computational calculations were performed using Gaussian 03 .[33] The DFT basis set B3LYP/6-31G(D,P) was chosen since it is expected to give reasonable results for intermediate size molecules and anions. The PCM solvation model for water was used.

Supporting Information Available: Olmstead–Nicholson technique for the second-order, bimolecular hydrogen generation reaction; Nicholson–Shain diagnostic criteria for pyridinium-catalyzed reduction of CO₂; comparison of simulated and experimental CVs for 4-*tert*-butylpyridinium in the absence and in the presence of CO₂ and for the catalyzed reduction of formic acid and formaldehyde; comparison of simulated and experimental CVs for the direct reduction of formic acid and formaldehyde; XPS spectra showing the electrode surface before and after bulk electrolyses; and CVs for the direct reduction of CO₂ at Pt. This material is available free of charge via the Internet at http://pubs.acs.org.

(57) Shirley, D. A. *Phys. Rev.* **1972**, *135*, 4709–4712.

JA1023496